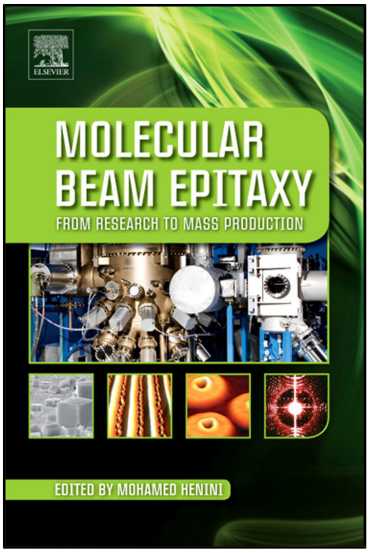

From Umansky V, Heiblum M. MBE growth of high-mobility 2DEG. In: Henini M, editor. Molecular Beam Epitaxy: From research to mass production. Elsevier Inc., 2013. p. 121–137.
ISBN: 9780123878397

Chapter 6

MBE growth of high-mobility 2DEG

V. Umansky and M. Heiblum

Department of Condensed Matter Physics, Braun Center for Submicron Research, Weizmann Institute of Science, Rehovot, Israel

Chapter Outline

6.1 INTRODUCTION

It is fair to say that the molecular beam epitaxy (MBE) technique revolutionised the semiconductor field and in particular in the scientific arena. This, far from equilibrium technique, allowed a construction of artificial structures, with atomically abrupt and flat interfaces, which do not exist in nature. What one could only draw on paper as a desired energy band diagram can now be realised with the greatest precision in the laboratory, constricting the world to two and one dimensions with atomic-like confinement that leads to energy quantisation. Tunnel barriers, quantum wells, resonant tunnelling devices, superlattices and alike became ubiquitous structures. Materials with different lattice constants were lured, via different kinds of growth techniques, to condense epitaxially on top of each other with a minimum number of defects, thus giving rise to a large variety of heterostructures. In extremely pure grown materials, electrons are found to zip along many microns without observable scattering events, exhibiting, e.g. quantum interference, which was thought before being observed only in the molecular, atomic and subatomic scales. Other effects, such as the quantum Hall effect (QHE), deeply rooted in the quantum regime of highly interacting electrons in two dimensions, were discovered unexpectedly. The rich world of mesoscopic physics emerged, spilling over to a vast number of applications. Commercial field effect transistors are routinely grown now by MBE, with high-mobility electrons confined to two dimensions below the surface of the structure. In addition, numerous optoelectronic devices, such as quantum well lasers with increased efficiency and improved wave-guiding due to confinement, have been developed.

In this chapter, we confine our discussion to MBE growth of high-purity AlGaAs–GaAs heterostructures embedding two-dimensional (2D) electron systems, which became the backbone of mesoscopic physics. Driven by the desire for a high-gain field-effect transistor (FET), it was advantageous to embed the electrons close to the surface in order to maximise the device's transconductance; very much like the

Molecular Beam Epitaxy. http://dx.doi.org/10.1016/B978-0-12-387839-7.00006-3

Molecular Beam Epitaxy, First Edition, 2013, 121–137

predecessor device, the silicon metal−oxide−semiconductor FET (MOSFET), where 2D electrons were confined at the interface of $Si-SiO_2$ via an applied electric field. In general, the confining potential quantises the energy of the 2D electrons, which tend to occupy only the lowest subband in the higher-mobility samples. Even though the electrons in silicon are rather heavy, and their mobility is not exceedingly high, the integer QHE had been discovered in such a MOSFET [1]. The lighter electrons, confined to the interface of a lattice-matched AlGaAs−GaAs heterojunction, were found to be a better structure for fundamental research [2]. On the one hand, the lattice-matched crystalline material (lattice mismatch between AlAs and the GaAs is ~0.1%), with very few interface states, hosts high-mobility electrons, but, on the other hand, the relatively low conduction band discontinuity in AlGaAs-GaAs and absence of suitable low interface trap density dielectric make it often difficult to form a two-dimensional electron gas (2DEG) electrostatically. Therefore, electrons are generally supplied via doping the AlGaAs layer; hence dubbed 'modulation doped' heterostructures. In these structures, the electron maximum mobility had rocketed from an initial ~20,000 $cm^2/V\,s$ to nearly $36 \times 10^6\ cm^2/V\,s$ today [3,4], with a fraction of a millimetre elastic mean free path. An outstanding mobility of holes, $\sim 2.6 \times 10^6\ cm^2/V\,s$, was also reported in the AlGaAs−GaAs system, enabling research with a hole system, where interactions are more readily dominant [5]. Remarkably, electrons in AlGaAs−GaAs heterostructure still possess the highest mobility among numerous competitor systems.

We aim here to cover the most important aspects of high-mobility MBE growth, including the main principles of system design (Section 6.2) and the strategy of the growth process (Section 6.5). It all emanates from understanding the main scattering mechanisms, which always play a pivotal role in all structures. We describe in Section 6.3 a few theoretical models that were developed in the 80's and 90's and demonstrate that despite the fact that these models failed to predict realistic values of the electron mobility, the derived functional behaviour agrees rather well with experiments, thus allowing us to distinguish among different scattering processes.

Modern mesoscopic physics covers a wide range of quantum phenomena that are observed in 2D systems. For example, typical transport experiments are interference of electrons under different conditions; shot noise measurements that reveal the value of the charge and its statistics; high-frequency measurements that access the time domain; local probe measurements that access the nanospatial dimensions; etc. Each of these studies necessitates an optimised structure, and in Section 6.4 we discuss the main considerations that are typically employed.

The value of the low-temperature mobility often constitutes merely a precondition for successful mesoscopic structures but does not guarantee obtaining the desirable behaviour, which is expected in an extremely pure material. One must keep in mind that while we strive for nearly perfect materials, most of the interesting physics rely on the presence of disorder. As an example, the QHE, while necessitating a rather pure material, cannot condense into the desired state in disorder-free 2D systems [6]. Consequently, the detailed character of the disorder is of prime importance. Indeed, as has been reported on several occasions, neither the mobility nor the single particle scattering time were found to be proper figures of merit for distinct and robust fractional QHE states [3,7−9]. The dependence on the details of the disorder, which we discuss in Section 6.6, is not fully understood and we believe that it requires a new approach towards 'disorder engineering'. Introducing impurities, as a source of carriers, is likely to add a conducting channel in parallel with the two-dimensional electron gas. Nature was kind by forming deep states and nonmobile carriers via the so-called DX centres [10] when Si is introduced as a dopant into the AlGaAs layer. This phenomenon allows the fabrication of highly stable gated mesoscopic devices; however, the resultant random potential in 2D often prevents the formation of fragile QHE states; thus, careful heterostructure design as well as 'disorder engineering' are necessary to smooth the potential fluctuations.

While most of the observed phenomena in coherent electron systems can be explained by 'single-particle' behaviour, many, due to electron interactions, which cannot be predicted a priori, are likely to be found as disorder weakens. Hence, the effort to grow nearly perfect materials will continue. Since the entry point, due to the mounting costs and the required expertise, is quite high, progress may be slow. In the following chapter, we try to simplify the 'magic of high purity growth' and with that hope to encourage new players to enter the field.

6.2 HIGH-MOBILITY MBE SYSTEM

The term 'molecular beam epitaxy' (MBE), introduced in 1970 by A. Cho [11], describes a process of epitaxial crystal growth that is facilitated as a result of atomic and/or molecular beams propagating in vacuum and condensing on a heated crystalline surface. The growth relies on kinematic processes on the surface, such as migration, adsorption, desorption, dissociation, and incorporation. Clearly, the process of growth requires real-time in situ monitoring and control, to assure the stoichiometry of the epitaxy. The MBE system is composed of a few ultra-high vacuum chambers with means for sample transfer between the different chambers, and one growth chamber. The latter is equipped with appropriate pumping facilities and various characterisation tools, sources of molecular or atomic beams, each functioning either by evaporation or

sublimation, and a substrate manipulator with a heater and a rotatable wafer holder. The basic design of an MBE system is described in detail in numerous manuscripts and textbooks (see for example Ref. [12–14]); hence, hereafter we limit our discussion only to specific aspects that must be addressed in a high-mobility MBE system.

6.2.1 Main principles of system design

The slimmest configuration of an MBE system includes a growth chamber, a buffer chamber and an introduction chamber, with the vacuum level improving progressively towards the growth chamber. This compartmentalisation allows moving a sample into and out of the growth chamber in a matter of hours, yet allowing the growth chamber to stay under ultra-high vacuum (UHV) for extended periods of time (often a few years). A wafer loaded into the introduction chamber is being preheated to drive the water off, outgassed in the buffer chamber at 350–400 °C and then introduced into the growth chamber for oxide removal at substrate temperature 580–620 °C under arsenic flux. Growth is then initiated under optimal conditions depending on the heterostructure design. More advanced systems include substrate thermal treatment in a separate outgassing chamber, while the buffer chamber is used to store prepared or already-grown wafers. Other substrate preparation methods, such as oxide blow-off with a hydrogen atom-beam source, have never been reported in a high-mobility MBE system – most probably due to concerns of additional sources of contamination (tungsten heater filament used for molecular hydrogen dissociation operates at 1800–2200 °C).

The most distinct feature of high-purity MBE machine is the use of extremely high-speed vacuum pumps in the growth chamber. While in early MBE systems ion pumps were quite standard, cryopumps today, though containing charcoal, are customarily used due to their high pumping speed and efficiency in pumping water vapour and other heavy and light gases. Often, a special design of large diameter cryopumps is employed including an additional liquid nitrogen (LN_2) cooled stage, which permits bakeout of the outer body of the pump at ~200 °C whilst the cryopump is operating [15]. Pumps containing a third stage, cooled close to the liquid helium temperature, are sometimes employed too [16]. Since the pumping speed is limited by the diameter of the pump, large UHV gate valves are needed to isolate the pumps from the chamber. It is preferable to use all-metal gate valves; however, their availability in large diameter is limited and their price is high. All metal parts inside the growth chamber, including those of the characterisation tools (ion gauges, residual gas analysis (RGA) sensor, etc.), which might be heated above room temperature during system operation, should be made from high-purity refractory metals. Using copper-free electrodes for filament welding might be also a worthwhile precaution. Insulators that protect electrical wires and thermocouples should be made of pyrolytic boron nitride (PBN), which has been thoroughly outgassed. Sapphire viewports are preferable to other types and are easier to bake at high temperatures. The LN_2 shroud should minimise cross-talk between effusion cells and has to be designed in such a way as to allow turbulence free motion of the liquid without gas pockets to assure uniform cooling of the internal surface walls. In contrast to early MBE systems, nowadays different types of effusion cells are employed for different materials. Conventional effusion cells are used for evaporation of gallium and aluminium (though they might have two filaments to provide temperature gradient along the cell), while several types of cracker cells were designed for producing the arsenic flux [17]. For dopants (silicon for n-type and carbon for p-type), either small size effusion cells or directly heated filament-like sublimation sources are used. When properly designed, the latter exhibit lower outgassing rates and faster thermal response compared to standard effusion cells. The cells, being the hottest parts of the system, should be constructed without internal virtual leaks and with the PBN crucibles and insulators of the highest possible purity. High-purity molybdenum (or tantalum) substrate holders are used with either direct radiative heating of the wafers or the wafers being mounted on the holder using indium (or gallium) as a solder. It is customary to utilise small wafer diameter (usually 2″) to minimise heater outgassing rate during growth. There is, however, no consensus regarding the optimal size of the effusion cells, particularly the gallium cell. In principle, for two effusion cells with a similar length, the ratio of the source flux to that of the residual impurities emanating from the cell (from its filament(s), crucible and tantalum shields) should increase with the cell diameter since at a certain temperature the source flux is proportional to the cell's opening area, while the effective emitting area of the impurities increases linearly with the diameter. In practice, however, several researches obtained better results with a smaller size Ga cell; yet, direct comparison is problematic and has never been reported.

The essential characterisation tools include reflection high-energy electron diffraction (RHEED), a sensitive RGA system, vacuum ion gauge(s), and beam flux detector (customarily designed nude gauge). The RHEED system, being absolutely necessary, at least in the initiation processes, necessitates two large openings in the cryopanel close to the wafer, which may lower the local pumping speed and introduce contaminations. Using aluminium-coated phosphorus screen for the readout may lower its outgassing.

6.2.2 Pregrowth system preparation

The MBE system works under extreme conditions: effusion cell temperature may reach ~1200 °C, internal walls are

cooled by liquid nitrogen, and the substrate, during rotation, may be heated up to more than 700 °C. Hence, every part of the system should stay always cold during the growth process or go through an outgassing process at high temperatures if it is hot during the growth. Cell shutters, adjacent areas to ion gauges, remote parts of the substrate manipulator and alike, are difficult to clean via local heating; thus, they should be a part of a prolonged bakeout at elevated temperatures. One has to make sure that all surfaces of the chamber, including those of the pumps, are heated uniformly to ~200–250 °C. A small segment that is left relatively cold during the bakeout cycle will later be dominant in outgassing if it is not properly cooled. It is advisable to use the RGA to monitor the chamber's environment during the bakeout cycle; it will be the determining factor in terminating the bakeout process. Effusion cells should be baked at a high temperature (~1600 °C) without the PBN crucible, and, if possible, in a different chamber, and later, again, with the PBN crucible in the cell, however, at a somewhat lower temperature (<1500 °C), to minimise PBN decomposition. Cells' shutters should be outgassed at the highest possible temperature (in a separate chamber or by the effusion cells themselves). Gauge filaments and substrate heater have to be heated for prolonged times at high filament current.

Needless to say, the starting source materials are the most important elements in high-quality epitaxial layers. The best MBE system will not remedy the consequence of an impure material. At this point, however, research groups rely mostly on commercial companies and no attempts to perform an additional purification process have been reported. During charging of the effusion cells, care should be taken to minimise oxidation of the source materials. Some researchers are using large plastic bags pressurised with pure argon tightly connected to the cells' ports during material loading. After the bakeout of the whole system, the materials should be carefully outgassed at temperatures above growth temperatures (with about ten times higher flux than the normal one). The preparation can be considered successful if a vacuum level of the order of 10^{-12} Torr is achieved while the effusion cells idle. Normally, no trace of gases other than H_2 and CO (with partial pressure at low 10^{-13} Torr) should be detected.

6.3 SCATTERING MECHANISMS IN 2D ELECTRON SYSTEM

6.3.1 Formation of 2DEG in modulation-doped structures

The introduction of modulation doping (MD) in 1978 [2], which employs the concept of spatial separation between ionised (parent) donor impurities and the electrons in the 2D electron system, is one of the outstanding examples of

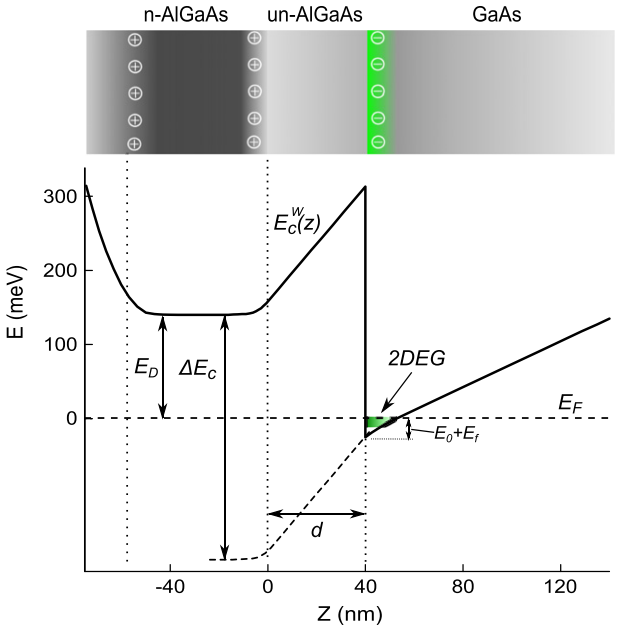

FIGURE 6.1 Profile of the conduction band minimum calculated self-consistently for modulation doped $Al_{0.35}Ga_{0.65}As$-GaAs heterostructure with deep DX centers and spacer thickness $d = 40$ nm (For colour version of this figure, the reader is referred to the online version of this book).

bandgap engineering. Figure 6.1 illustrates schematically the formation of 2DEG near the heterointerface between the wide bandgap AlGaAs and the narrow bandgap GaAs. Intentionally doping the AlGaAs and pinning the Fermi level at the donor energy level E_D result in an intrinsic electric field in the undoped regions, with the conduction band energy $E_c^W(z)$ rising in the AlGaAs. Furthermore, in the narrow-gap (undoped) material, placed at some distance d (spacer) from the doped layer, a triangular-like quantum well filled with electrons is formed as long as the conduction band discontinuity ΔE_c is larger than $E_c^W(z)$. The density of the 2DEG n_s can be calculated in the ubiquitous, simplified case of δ-doping (a single sheet of dopant atoms), at low-temperature and for a single occupied subband:

$$n_s = \frac{\varepsilon\varepsilon_0}{q}\frac{(\Delta E_c - E_D) - [E_0(n_s) + E_f(n_s)]}{d} \qquad (6.1)$$

where the energy is measured from the Fermi level, ε is the dielectric constant of the semiconductor, ε_0 is the vacuum permittivity, q is the electronic charge, ΔE_c is the conduction-band discontinuity between that in the GaAs and in the doped AlGaAs region, $E_0(n_s)$ is the subband energy in the triangular quantum well, $E_f = n_s\pi\hbar^2/m^*$ is the chemical potential at $T \sim 0$ K and m^* is the effective mass of an electron. Numerical solution of Eqn (6.1) shows that for a wide range of electron densities $\sim 5 \times 10^{10}$–5×10^{11} cm^{-2} charge transfer is essentially defined by the energy difference $\Delta E_c - E_D$. While the

conduction band discontinuity for the AlGaAs–GaAs interface is known quite well, the position of the donor level is rather complicated, since most of substitutional group IV impurities in Al(Ga)As do not behave as simple shallow donors. Besides the shallow ionised donor state, the impurities also form negatively charged deep states, so-called DX centres. While in GaAs the DX centres are located high within the conduction band, and hence not felt, in AlGaAs they form the lowest-energy donor states in the gap when the AlAs mole fraction exceeds ~22%. Properties of DX centres should be taken into account for an optimum design of 2D systems, as will be detailed later.

An accurate determination of the areal electron density and the positions of the energy levels in the 2D quantum well for an arbitrary doping profile require a self-consistent calculation involving Poisson and Schrödinger equations, which can be found in a large number of publications. They involve different approximations; all, but a few, lead to the familiar Airy wavefunctions in the triangular well (see for example Ref. [18–20]). Nowadays, one can find software programs that provide rather accurate numerical solutions (1D, 2D and 3D); for example, Nextnano simulator developed in the Walter Schottky Institute.

6.3.2 Mobility of electrons in 2DEG

In semi-classical transport theory, the low-field conductivity is $\sigma = en\mu$, where the mobility μ is defined via $\upsilon_d = -\mu E$, with υ_d being the carrier drift velocity and E being the electric field. In turn, the mobility is related to the momentum relaxation time τ_m via $\mu = e\tau_m/m^*$. One can also define the elastic mean free path $l_e = \upsilon_F\tau_m = \mu\hbar\sqrt{2\pi n_s}/e$, where $\upsilon_F = \hbar k_F/m^* = \hbar\sqrt{2\pi n_s}/m^*$ and k_F is the wave vector on the Fermi surface. For low enough electric fields, electron scattering is elastic and the momentum relaxation time is weighted over the scattering angle θ; hence, the large angle scattering dominates:

$$\frac{1}{\tau_m} = \frac{1}{2\pi}\int_0^{2\pi}\frac{1}{\tau_i}(1-\cos\theta)\mathrm{d}\theta \qquad (6.2)$$

The low-temperature electron mobility, being a direct estimate of the elastic mean free time, is commonly regarded as the 'figure of merit' for the 2DEG. It is determined easily by measuring the conductivity and the carrier density. With the discovery of modulation doping, a large number of theoretical papers attempted to calculate the influence of different scattering processes on the electron mobility [21–28]. It should be noted that the majority of these calculations agreed rather well with the experimental results available at the time of the publications; however, they failed to predict realistic values for much longer scattering times in high-mobility 2DEG. Recently, Das Sarma and Hwang [29], encouraged by the record electron mobility exceeding $35 \times 10^6\,\mathrm{cm^2/V\,s}$ reported by several groups [3,4], employed more accurate numerical calculations to suggest that the only factor limiting electron mobility in AlGaAs–GaAs heterostructures is the purity of the undoped GaAs. A mobility of $\sim 100 \times 10^6\,\mathrm{cm^2/V\,s}$ at carrier density of $3 \times 10^{11}\,\mathrm{cm^{-2}}$ is possible provided that the unintentional ionised impurity concentration in GaAs is lowered to $10^{12}\,\mathrm{cm^{-3}}$. Nevertheless, understanding the following scattering mechanisms is of great importance for realisation of high-mobility 2D systems:

i. Unintentional charged impurities in GaAs;
ii. Intentional ionised donors in the AlGaAs layer;
iii. Interface roughness of the AlGaAs–GaAs heterointerface;
iv. Alloy scattering in the AlGaAs spacer;
v. Acoustic phonons (via deformation potential & piezoelectric coupling).

Other scattering mechanisms, such as longitudinal optical phonon scattering and short-range scattering by neutral defects and neutral impurities, were shown to have only a minor influence on the mobility [29]. Let us discuss each of the scattering contributions separately.

6.3.2.1 Scattering by unintentional charged background impurities in GaAs (BG)

The mobility μ_{BG} is inversely proportional to the impurity concentration (N_{BG}); however, it increases with electron density due to screening $\mu_{\mathrm{BG}} \propto n_s^{\delta} N_{\mathrm{BG}}^{-1}$, where the value of δ is still being debated. While Gold [27] found $\delta \sim 0.8$ for $n_s = (0.1-1) \times 10^{11}\,\mathrm{cm^{-2}}$, Das Sarma and Hwang [29] showed that δ strongly depends on electron density, with $\delta = 0.5-1.1$ for densities $(0.5-3) \times 10^{11}\,\mathrm{cm^{-2}}$. In experiments, where the density is varied either by a controllable illumination or by applying an external electric field, $\delta = 0.6-1.0$ was observed [15,16,30,31]; however, a modified screening environment influences also other scattering mechanisms, making accurate determination of δ difficult.

6.3.2.2 Scattering by intentional remote ionised donors (RI)

For delta doping in the AlGaAs, with areal density N_{RI}, located at a distance d from the AlGaAs–GaAs interface, the theory predicts a sharp dependence of the mobility μ_{RI} on d ($\mu_{\mathrm{RI}} \propto d^3$) for relatively thick spacers i.e. $k_F d \gg 1$. Screening increases the RI mobility with an approximate dependence $n_s^{1.5}$ in the density/spacer range relevant to high-mobility systems [29], leading to $\mu_{\mathrm{RI}} \propto d^3 n_s^{1.5} N_{\mathrm{RI}}^{-1}$. Furthermore, taking into account the fact that the 2DEG areal density itself depends on spacer thickness (being

almost inversely proportional to it at relatively thick spacers) and calculating the limiting mobility for $N_{RI}^{min} \approx n_s$ (this may be achieved by using a large distance between the interface and the surface or utilising multiple doping schemes), one finds a limiting RI mobility dependence on the spacer thickness to be $\mu_{RI} \propto d^{2.5}$.

6.3.2.3 Interface roughness scattering at the AlGaAs–GaAs heterointerface (IR)

Being a rather controversial issue, this mechanism has been suggested on several occasions to lead to the anisotropy of the mobility in the interface plane. However, since the interface roughness may depend on growth details, AlAs mole fraction and substrate orientation, it has been difficult to ascertain its universality. Moreover, an experimental observation of IR scattering is very problematic, since first, distinguishing between IR scattering and alloy scattering is not easy, and second, several other effects, such as parallel conductance in the doped layer, gate leakage and second subband occupation, may mask the intrinsic IR scattering. Most theoretical treatments are based on the pioneering work of Ando [21], who applied the theory developed for the Si–SiO_2 interface to the AlGaAs–GaAs heterointerface, concluding that interface roughness scattering may be important only at high electron densities (~10^{12} cm^{-2}). With increasing carrier density an almost linear drop of the interface roughness scattering limited mobility was predicted [32]; thus, it is expected that the contribution of IR scattering should lead to saturation or even a drop in the measured electron mobility at high electron density. Such behaviour was indeed observed in several studies [9,33], while others reported only on a monotonous dependence of mobility on density following a single positive exponent $\mu \propto n^{\delta}$ behaviour [16,34,35].

6.3.2.4 Alloy scattering in the AlGaAs spacer

With the electron wave function penetrating into the AlGaAs (with an exponentially small tail), short-range disorder, due to the random nature of the alloy, is always present. The limiting mobility is expected to be inversely proportional to the carrier density [22,25]. Without credible experimental evidence, the common consensus is that alloy scattering is irrelevant in limiting the mobility.

6.3.2.5 Acoustic phonon scattering

This mechanism sets the ultimate mobility limit at any temperature [29,36]. Since the scattering rate falls quickly with temperature, at approximately $T < 1$ K it becomes irrelevant and the temperature-independent ionised impurity scattering rate becomes dominant (Figure 6.2).

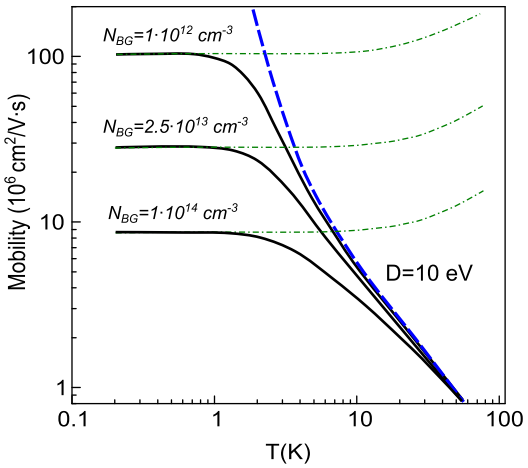

FIGURE 6.2 Calculated electron mobility (black lines) as a function of temperature for different background impurity densities. Electron density and spacer thickness were fixed at $n = 3\times10^{11}$ cm^{-2} and $d = 120$ nm. Acoustic phonon scattering limited mobility (dashed line) was calculated using a deformation-potential coupling constant $D = 10$ eV. The upper mobility limit is set by charged impurity scattering (dot-dashed lines) (For colour version of this figure, the reader is referred to the online version of this book). Source: *Courtesy of Das Sarma & Hwang.*

6.3.3 Comparison with experiments

Though the theoretical models usually fail to predict accurately the correct values of the mobility, they still may aid in assessing the relative contribution of each scattering mechanism, as seen in the example shown in Figure 6.3a. There the mobility was measured in a set of $Al_{0.35}Ga_{0.65}As$/GaAs samples with a spacer thickness in the range of 20–150 nm, 15 nm uniformly doped $Al_{0.35}Ga_{0.65}As$ layer and undoped 17-nm-thick cap layer. The doping density was kept at a minimum that is necessary to supply the electrons to the 2DEG and to compensate the surface states. The mobility was measured in the dark, after brief illumination with infra-red LED. The experimental data were fitted using the functional dependences of the remote and background ionised impurities employing the Mathiessen rule:

$$\frac{1}{\mu}\left(\frac{\mathrm{V\ s}}{\mathrm{cm}^2}\right) = \frac{1}{\mu_{BG}} + \frac{1}{\mu_{RI}} \approx \frac{1}{21\times10^6}\left(\frac{d}{70\ \mathrm{nm}}\right)^{0.7} + \frac{1}{92\times10^6}\left(\frac{d}{70\ \mathrm{nm}}\right)^{-2.5} \quad (6.3)$$

Here the spacer thickness is normalised to 70 nm, which was the "optimal" spacer thickness d^*. The relative contribution of the remote impurities scattering rate to the total one μ/μ_{RI} was also calculated using Eqn (6.3) and is shown in Figure 6.3b.

The experimental data seem to fit rather well the theoretical expectations at a temperature where phonon scattering is negligible. It may be worth noting the following:

- For relatively thin spacers, $d < 30$ nm, the mobility is limited by remote ionised impurities; while in the

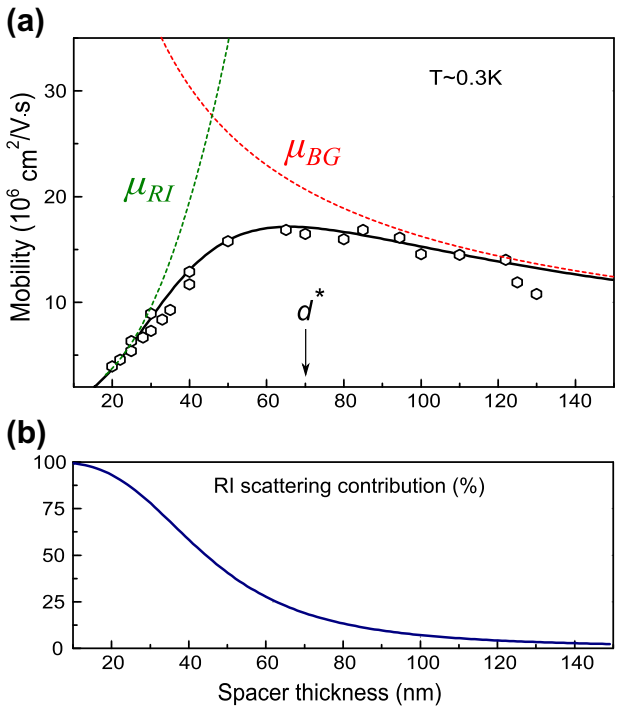

FIGURE 6.3 (a) Calculated dependence of electron mobility on spacer thickness (solid line) fitted to the experimental data measured in 2DEG samples with $Al_{0.35}Ga_{0.65}As$ spacer, a uniformly doped 15 nm wide $Al_{0.35}Ga_{0.65}As$ layer, capped by an undoped 10 nm thick $Al_{0.35}Ga_{0.65}As$ layer and 7 nm thick GaAs layer. (b) The relative contribution of the remote ionised impurity scattering calculated from the corresponding limited mobility curves (For colour version of this figure, the reader is referred to the online version of this book).

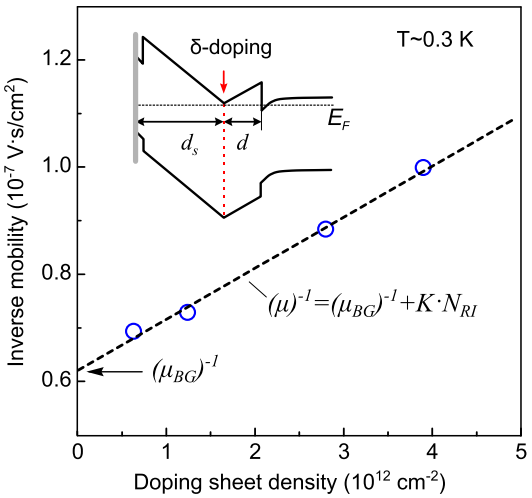

FIGURE 6.4 Inverse electron mobility, measured in the dark after illumination, as a function of doping sheet density in a set of samples with spacer thickness $d = 72$ nm and a variable distance from the doping layer to the surface. The inset shows a schematic band diagram of the structures used in this experiment. The extrapolated linear fit (dashed line) reveals background impurity limiting mobility as ~16×10^6 cm^2/V s (Ref. 16) (For colour version of this figure, the reader is referred to the online version of this book).

opposite limit, $d > 100$ nm, the mobility is almost entirely determined by the BG scattering;

- The mobility has a maximum at an "optimal" spacer thickness d^*, with the contribution of BG scattering clearly prevailing;
- The mobility limited by the background ionised impurities was used to estimate the unintentional p-type background impurity density to be ~$(1-2) \times 10^{13}$ cm^{-3} (by comparison with known data for low mobility systems, where background concentration is known).

Obviously, besides the spacer thickness, the total depth of the 2DEG below the surface also influences the relative contribution of RI scattering and, thus, mobility. Indeed, in shallow structures, the pinning of the Fermi level by the surface states necessitates higher doping levels causing an additional scattering.

A more accurate method to distinguish between the different scattering mechanisms was suggested by us in Ref. [16]. The method involves plotting the inverse mobility for a set of single delta-doped heterostructures with the same spacer thickness as a function of ionised donor density (Figure 6.4). The doping (N_{RI}) and distance to the surface (d_s) were varied to establish nearly full donor ionisation after illumination, but yet provide the same equilibrium electron density. The background impurity-limited mobility was determined by extrapolation for $N_{RI} \to 0$, thus allowing calculating the relative contribution of RI scattering for samples with different total 2DEG depth and also illustrating that in 2D systems without a limitation on the total depth, the influence of RI scattering can be minimised.

6.3.4 Correlations among ionised impurities

An additional factor, which may influence the mobility, is a possible spatial correlation among the ionised impurities. Indeed, in an ideal case, if all the ionised impurities would be placed in a periodic manner, RI scattering would be virtually eliminated (new energy bands, though, will be formed). In reality, since the dopant placements are random, correlation among the ionised donors may arise only when their density exceeds the number of ionised impurities at equilibrium [37]. This phenomenon was first observed in 3D semiconductors [38] and later reported for 2DEG in AlGaAs–GaAs heterostructures [39–41]. The degree of correlation obviously depends on the ratio N_D/N_{RI} (N_D is the donor density) and on the freeze-out temperature of electrons in the doping layer; hence, a proper structure design and doping scheme may facilitate effective spatial correlations among the ionised donors.

6.4 DESIGN OF HIGH-MOBILITY 2DEG STRUCTURES

Electrons can also be induced electrostatically without modulation doping, thus avoiding much of the RI scattering. However, several attempts to accomplish this either by utilising various types of surface gates [42–44] or by using n^+-doped GaAs back gate [45] resulted in inferior electron mobility in comparison with the "standard" modulation-doped heterostructures. While the cause of this behaviour is not fully understood, it had been pointed out that charged surface states (Schottky states) may act as remote scatters, especially when metal gates are employed [42]. In modulation-doped systems, however, the doped layers, placed between the 2DEG and the surface, may be effective in screening the charged surface states.

Hereafter, we consider the most important design aspects of modulation-doped heterostructures. The desired structure must fulfil the requirements of the experiment, such as areal density of electrons, low-temperature mobility, and total depth below the surface. These requirements are not necessarily complementary. For example, high-mobility electrons require thick spacer with large total depth below the surface. However, the large depth makes it difficult to obtain reliable ohmic contacts and limits the lateral dimensions of confining potentials in quantum mesoscopic devices.

6.4.1 Buffer layer

The buffer layer, separating the active layers from the substrate, must fulfil three basic functions:

- **i.** Since even the most meticulous substrate preparation cannot provide atomically smooth surface, which becomes even rougher during the initial 'oxide blow-off', the buffer layer facilitates a smooth interface for the 2D electrons;
- **ii.** Impurities that are inevitably present in and on the substrate (due to ex situ processing) tend to migrate towards the epitaxial layers during the growth process. Growth of a relatively thick buffer layer, which in many cases contains AlGaAs–GaAs superlattice (SL), was shown to retard impurities from migrating due to the high chemical reactivity of the aluminium-containing layers. Moreover, it was also shown in numerous reports that a properly chosen SL leads to a significant smoothing of the surface during the growth;
- **iii.** In most cases growth is performed on semi-insulating (SI) GaAs substrates, with the Fermi level pinned in mid-gap due to an abundance of mid-gap traps in the substrate. This pinning gives rise to an electric field that penetrates as far as the AlGaAs–GaAs interface (the depletion region in a typical buffer layer may exceed 3 μm), lowering the 2DEG areal density, and hence, necessitating a rather thick buffer layer. Instead, adding a n^+ doped layer near the substrate–buffer interface can partly compensate this electric field and allow a thinner buffer layer. Obviously, the 'compensating' doping density should be chosen low enough to ensure full ionisation of dopants, thus, avoiding a parallel conductance path.

6.4.2 Spacer layer

The spacer thickness and the energy difference $\Delta E_c - E_D$, with ΔE_c in the doped region, determine the 2DEG areal density. Despite the fact that the AlAs mole fraction in the undoped spacer and doped layers is chosen ubiquitously to be the same, it could be designed to vary gradually in the spacer region without notable influence on the areal electron density. For example, in high-mobility structures it is often advantageous to use a relatively low AlAs mole fraction near the interface in order to improve the interface roughness as well as to decrease outgassing of the Al cell shutter during the growth of the GaAs channel. In structures where doping is introduced on both sides of the confined 2D channel, particular attention must be paid to the lower spacer, since its 'inverted interface' with GaAs tends to be rougher. In this case a short-period superlattice is a preferable option for the bottom spacer.

6.4.3 Doping efficiency and DX centres

The doping layer constitutes the most important element of modulation doped system. Silicon has been proven to be an optimal n-type dopant due to its relatively low diffusivity and high degree of activation. Moreover, Si plays a role of both shallow and deep (DX) donor states, with the latter often being beneficial when freeze-out of electrons in doped region is desirable (preventing parallel conductance and improving device stability). The properties of DX centres have been studied since their discovery in the 70s [46,47] accompanied by a large volume of publications summarised in several reviews and textbooks [10,48]. Here we briefly discuss their behaviour that is relevant in high-mobility structures.

The accepted model of DX centres, confirmed by numerous experiments (see for example Ref. [49]), is that the Si atom moves from its substitutional position in AlGaAs (replacing Ga or Al) while capturing an additional electron from one of its neighbouring Si atoms, thus producing a negatively charged DX^- centre and a positively charged ionised donor D^+. The relative average distance between the ions DX^- and D^+ with respect to the spacer thickness, as well as possible correlation in the ionised Si atom positions, determines the contribution of

such $D^+ - DX^-$ 'dipoles' to the scattering process. Mobility was found to increase only modestly due to spatial correlations among the DX centres, most probably due to their high freeze-out temperature [39–41].

Three energies characterise a DX centre: capture energy, emission energy and the donor level, namely, its energy relative to the bottom of the conduction band at equilibrium (E_{DX}). There are multiple deep donor states, each corresponding to the number of neighbouring Al atoms near the Si atom (zero, one, two or three). Every state has its occupation probability, characteristic energies and a capture cross section depending on the AlAs mole fraction (x). However, in most cases it is sufficient to regard the Si donor as a single (average) DX state with a linear dependence of its energy below the bottom of the conduction band (following the evolution of the L band in the AlGaAs), starting from zero at $x \sim 0.22$ and reaching ~0.16 eV at $x \sim 0.4$, where the AlGaAs becomes an indirect semiconductor (Figure 6.5). The large emission and capture energies result in electron freeze-out at temperatures as high as 120–140 K. Illumination by light with photon energy higher than the emission energy converts the deep DX^- centre to a $D^+ + 2e$, with the Fermi energy pinned to the shallow donor state, thus leading to a substantial increase in areal electron density (and the mobility). This effect is often referred to as persistence photoconductivity [47].

The presence of DX centres affects the doping efficiency, which is the maximum 2DEG areal density for a certain spacer thickness. Indeed, as can be seen in Figure 6.5, the energy difference $\Delta E_c - E_{DX}$ is notably smaller in comparison with that of shallow donors, thus reducing the electron density. Raising the AlAs mole fraction in order to increase ΔE_c leads to a modest increase in the electric field in the spacer, since ΔE_c changes as

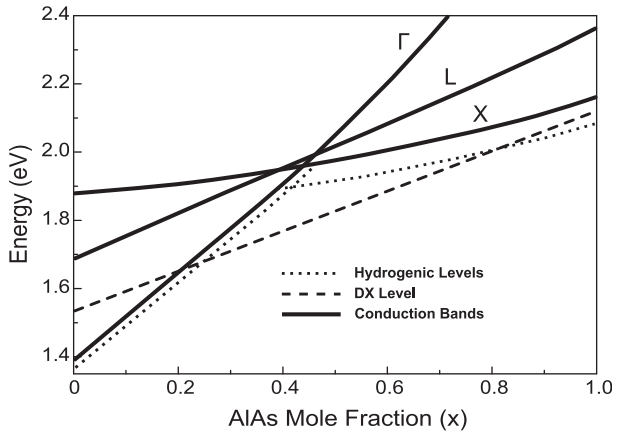

FIGURE 6.5 A schematic diagram of the main three conduction band minima in AlGaAs, the shallow donor levels (dotted), and the DX level (dashed) as a function of the AlAs mole fraction. Source: *Adopted from the Ref. 10.*

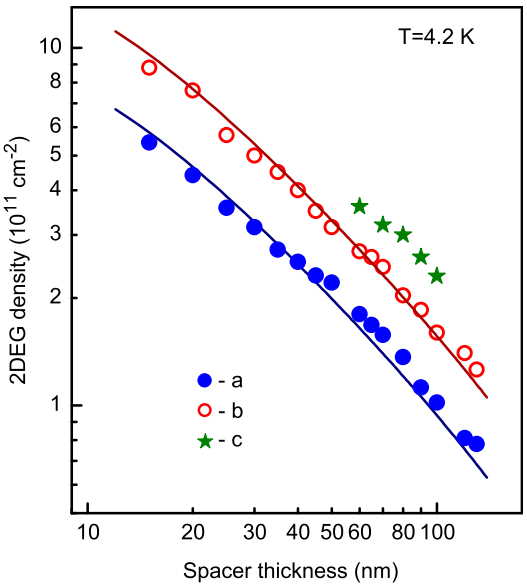

FIGURE 6.6 The dependence of the areal electron density on spacer thickness in $Al_{0.35}Ga_{0.65}As$-GaAs δ-doped heterostructures at T = 4.2 K: (a) measured in the dark; (b) measured in the dark after illumination. Theoretical curves (lines) were calculated self-consistently with the following parameters: background impurity density 2×10^{13} cm^{-3}, $\Delta E_c = 340$ meV, $\Delta E_{DX} = 120$ meV and $\Delta E_D = 6$ meV for a shallow donor level. (c) The electron density measured in the dark in Double Heterointerface Doped structures with 2DEG embedded in 30 nm wide QW and doping made inside a short period superlattice (see paragraph 6.4.4.4) (For colour version of this figure, the reader is referred to the online version of this book).

~0.98x eV for $x < 0.4$ (see Ref. [50]), while the DX energy changes as $E_{DX} \approx 0.9x$ eV (for $0.22 < x < 0.4$). The doping efficiency, however, increases normally by ~30–60% after illumination, exhibiting a much stronger dependence on the AlAs mole fraction. As an example, Figure 6.6 shows calculated and measured electron densities before and after illumination, as a function of spacer thickness in delta-doped $Al_{0.35}Ga_{0.65}As$–GaAs samples grown in our laboratory. Similar results were also reported by other groups (see for example Ref. [51,52]).

6.4.4 Doping schemes

6.4.4.1 Uniform vs. delta (δ) doping

Customarily the AlGaAs layer is doped either via evaporating Si atoms during a continuous growth process, dubbed 'uniform doping' (Figure 6.7a) or via evaporating a fraction of a Si monolayer during a growth interruption (with As over-pressure), dubbed 'δ-doping' (Figure 6.7b). In the latter, a slightly higher charge transfer is achieved, since the width of the depletion layer in the δ-doped region is negligible, making the effective spacer thickness smaller. Note that in order to get an extremely thin doped layer (a true δ-doping), the substrate temperature must be low

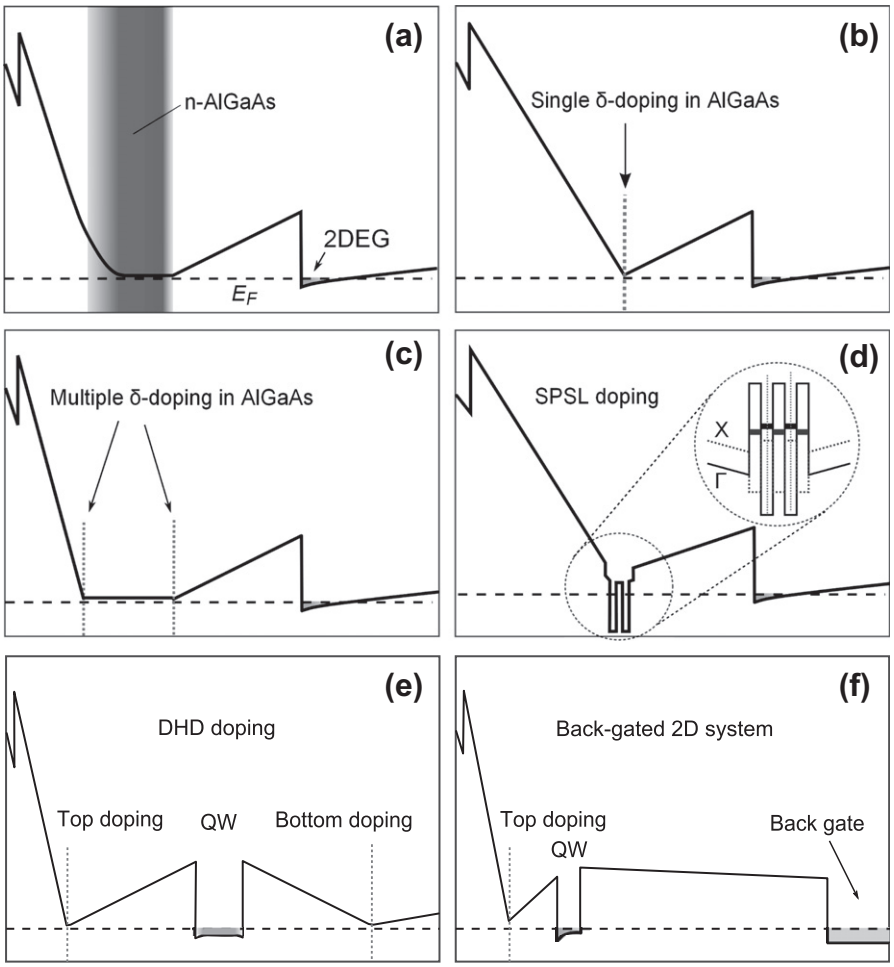

FIGURE 6.7 Conduction band minima profile in heterostructures with different doping methods. (a) Singe uniform doped layer. (b) Single δ-doped layer. (c) Two δ-doped layers, one supplying the surface states and one the 2D electron layer. (d) Single SPSL doped later. (e) δ-doping in DHD structure. (f) Single δ-doped layer above and N^+ back-gate below the 2D electron gas.

enough to avoid thermal diffusion and segregation of the Si atoms. The δ-doping method has become the industry standard for high-mobility transistors since it allows placing the 2DEG close to the surface, thus leading to higher transconductance. However, for gated mesoscopic devices, operating at deep cryogenic temperatures, uniform doping seemed to provide a better device stability (likely due to larger distance between impurities, which may prevent electron hopping).

6.4.4.2 Multiple doping schemes

Suggested first in Ref. [53], the multiple doping scheme allows separation between donors that supply electrons to the 2DEG and those providing electrons to the surface states (Figure 6.7c). This method, while increasing the depth of the 2DEG beneath the surface, minimises the number of ionised impurities near the 2D channel. Since the scattering rate drops approximately as the cube of the distance between the ionised impurities and the 2DEG, scattering from the upper doping layer is generally negligibly small. This scheme is often used in very high-mobility structures dedicated to studies of the fractional quantum Hall effect (FQHE). Obviously, both uniform doping and δ-doping may be used in various combinations in a single structure.

6.4.4.3 Short-period superlattice doping (SPSL)

The elegant and possibly the only way to avoid formation of DX centres is to introduce a δ-doping spike in a thin, confined, GaAs layer – being part of a short-period GaAs–AlAs superlattice (Figure 6.7d). Such doping scheme was first proposed by Baba et al. in 1983 [54], and further modified by Friedland et al. in high-mobility 2D structures [55]. The main idea is based on separating the Si atoms from the Al containing layers, thus preventing the formation of DX centres. Confining the doping in a thin quantum well (QW) quantises and raises the electron energy and thus allows charge transfer to the 2DEG. The thickness of SPSL layers is chosen to make it type-II superlattice, namely, with the ground state in the AlAs

layers (X_z – minima, where z stands for growth direction) being lower than that (Γ minimum) in the GaAs wells. Hence, excess electrons in SPSL, if any, will spill into the AlAs layer. The parameters that correspond to the type-I to type-II crossover in asymmetric $(GaAs)_m/(AlAs)_n$ SPSL (where m and n stand for the number of monolayers) are known rather well from numerous optical experiments (see, for example, Figure 2 in Ref. [56]). The electrons in the AlAs layers, being heavier than those in GaAs by a factor of ~3, are easily localised at cryogenic temperatures due to disorder in the SPSL. Charge transfer is governed by the quantised electron level in the SPSL independently of the AlAs mole fraction in the spacer layer. Most importantly, since the freeze-out temperature in the SPSL is low, spatial correlations among ionised donors are effective and scattering due to remote ionised impurities is significantly suppressed.

6.4.4.4 Double heterointerface doping (DHD)

In a symmetrical structure, the 2DEG resides in a QW with spacers and doping layers on both sides (Figure 6.7e). This structure was first introduced in 1985 by Hikosaka et al. for power AlGaAs–GaAs transistors [57]; however, it was not adopted by the high-mobility community, since the 'inverted' interface (GaAs on top of AlGaAs) limited the electron mobility due to higher interface roughness and Si segregation towards the GaAs channel. With a mobility of more than 30×10^6 cm^2/V s reported by Pfeiffer and West [58], the structure has been adopted for high-mobility 2DEG ever since.

The prominent feature of the DHD structure is the almost doubled 2D areal density compared with a single side-doped heterostructure with the same spacer thickness. This is illustrated in Figure 6.6, which shows the areal density as a function of spacer thickness in SPSL-doped DHD structures grown in our laboratory. The higher density improves screening and, hence, leads to a higher mobility. Indeed, according to the classical scattering models described in Section 6.3, the BG scattering mobility limit should increase by a factor of 2^δ ($\delta = 0.5$–1.1), while the limit due to RI rises by a factor of ~$2^{0.5}$ (since the number of ionised donors is also doubled). Obviously, the width of the QW has to be chosen carefully to obtain high electron density but avoid the occupation of higher sub-bands, which will open an additional scattering channel. For the most common well width of 30–40 nm and spacer thickness $70\ \text{nm} < d < 100\ \text{nm}$, the areal density is 3.0–3.5×10^{11} cm^{-2}. It should also be noted that interface roughness scattering, if any, is relatively weak in a symmetrically doped DHD, since the electron density profile peaks at the centre of the QW – away from the interfaces. Figure 6.8 illustrates the effect of doubling the electron density in DHD structures on the mobility with

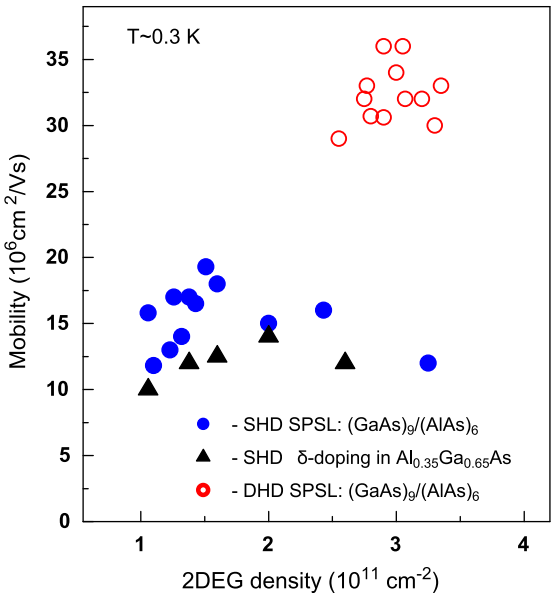

FIGURE 6.8 Low-temperature electron mobility measured in the dark at different electron densities and for different doping schemes. All the samples were grown in the same growth campaign (For colour version of this figure, the reader is referred to the online version of this book).

a comparison to high-quality single interface-doped (SHD) samples. The highest mobility in DHD structures is about 1.6–2 times larger than in the corresponding SHD ones with the same spacer thickness – very close to the theoretical limit accounting only for BG scattering, thus confirming the negligible contribution of other scattering mechanisms.

6.4.4.5 2D systems with back gate

This design allows varying the density of the 2DEG residing in a QW (Figure 6.7f). A back gate is employed either via an n-type GaAs substrate or via an n^+-GaAs layer grown on top of the buffer layer, both separated from the 2DEG by an AlGaAs barrier. The barrier should be designed to minimise back-gate leakage and enable low-resistance ohmic contacts to the 2DEG without shorting to the back gate. Back-gate design is clearly preferable to top gate approach (see for example Ref. [35]), since it affects the 2DEG density uniformly across the entire device area, in contrast to the top gate, which has to be laterally separated from the ohmic contacts, thus leaving ungated areas.

6.5 MBE PROCESS FOR HIGH-MOBILITY 2DEG

The fundamentals of the MBE growth process are rooted in intensive research on epitaxial growth of GaAs starting in 1970s with the pioneering works of Foxon and Joyce using modulated flux mass spectrometry and RHEED [59,60].

The resultant basics are described in great detail in numerous reviews and textbooks (e.g. Ref. [12,13,61–64]), which cover a wide range of applications and materials. Hereafter, we concentrate mostly on those aspects of the growth process, which are relevant for high-mobility 2D systems where the background impurity concentration as well as interface quality are the major concerns. We discuss the epitaxial growth on (100)-oriented GaAs substrates, since they are known to provide the highest mobility.

6.5.1 MBE growth of AlGaAs–GaAs heterostructures

The AlGaAs–GaAs system is nearly lattice matched; hence, heterostructures growth is easily accomplished with negligible mechanical stresses. There is a wide temperature 'window' ~500–650 °C where high-quality epitaxial GaAs layers can be grown by MBE, with the upper temperature limit being set by the congruent sublimation point (where the sticking coefficient of Ga becomes less than unity). While Ga is supplied as an atomic flux using a suitable effusion cell, arsenic can be produced in a form of either tetramer As_4 or dimmer As_2 molecules, with the latter formed by a thermal cracker cell. It was shown that the sticking coefficient of As_4 and As_2 in the useful temperature range is almost zero in the absence of gallium population on the surface; thus, the growth rate is ultimately determined by the impinging Ga flux (as long as its sticking coefficient remains near unity). While As_2 species incorporate by a first-order dissociative chemisorption on a surface covered by Ga atoms, the incorporation of As_4 molecules is a more complex, second-order process, involving two As_4 molecules. Four As atoms are chemisorbed on the growing surface and a residual As_4 molecule is desorbed, thus limiting the maximum sticking coefficient of As_4 to half. Another phenomenon determined by the thermodynamic equilibrium on the surface is arsenic desorption at temperatures above ~350 °C, which requires, for normal growth, a certain temperature-dependent over-pressure of arsenic to maintain the so-called 'As-rich' condition, since the 'Ga-rich' condition is usually quickly accompanied by formation of liquid Ga droplets on the growing surface. Optimising the growth parameters is accomplished by the aid of RHEED, via in situ monitoring of the surface reconstruction, which is indicative of the growth condition. For example, at temperatures above ~500 °C the As-rich surface exhibits (2×4) surface reconstruction that may gradually convert to Ga-rich (4×2) surface reconstruction if the substrate is being heated at a constant arsenic flux. The boundary lines between different surface reconstructions for different substrate temperatures and arsenic over-pressure yield the so-called surface phase diagram, either static (without group III element flux) or dynamic – studied for GaAs and AlAs in detail (e.g. Refs. [65,66]).

Growth of III–V alloys obeys similar mechanisms as those of GaAs, though, quantitatively the behavior may be different. For example, for the growth of AlGaAs alloy, the surface mobility of the Al atoms is several times smaller than that of Ga, necessitating a higher growth temperature, yet with a stable AlAs surface at high temperatures (up to ~795 °C in the absence of the arsenic flux [66]).

6.5.2 Growth process for high-mobility MD heterostructures

The MBE process for high-mobility 2D systems is based, to a great extent, on results that were obtained during almost two decades of extensive studies during 1970s–1990s, with comprehensive summaries in several reviews and textbooks (e.g. Ref. [63]). Since both the quality of the MBE system and the purity of the source materials have improved with time, some of the previous works are less relevant nowadays.

There are three major technological factors influencing the quality of high-mobility AlGaAs–GaAs structures: the growth temperature; the As/Ga(Al) beam fluxes ratio; and the growth rate. Proper choice of these parameters should allow achieving the following goals: (i) minimising unintentional impurity incorporation; (ii) achieving smooth surface/interface; and (iii) preventing undesirable diffusion and segregation of intentionally introduced dopants. The following sources of unintentional impurities should be considered in high-mobility UHV–MBE system:

- Imperfect vacuum environment in the growth chamber;
- Finite purity of the source materials (Ga, Al, As and to a lesser extent Si);
- Outgassing of heated parts (filaments, PBN parts, shutters, etc.).

It is well established, via sensitive low-temperature photoluminescence, that the main unintentional impurity in high-purity GaAs is carbon, with density below $10^{14}\,cm^{-3}$; however, its main source is not obvious. For instance, the increase of mobility with increased growth rate points out to the incorporation of impurities from the environment, which may result from a minute leak (real or virtual) or outgassing of substrate heater assembly. Alternatively, an absence of such dependence provides evidence that the main source of impurities is the effusion cells. In a well prepared and leak-tight MBE system, with a vacuum level better than 1×10^{-11} Torr the latter phenomenon is usually observed.

Carbon incorporation seems to depend strongly on the growth temperature and As/Ga beam flux ratio. For example, it was reported in Ref. [67] that decreasing the As_4/Ga beam flux ratio from 60 to 20 at a substrate temperature of 620 °C led to a 5 times lower photoluminescence peak

intensity associated with carbon impurities, while growing at lower temperatures results in an increased carbon incorporation and poorer surface morphology. Nowadays, the basic growth process of high-purity GaAs takes place at 630−650 °C, close to the congruent sublimation point, at a minimum As_4 flux, barely sufficient for As-stable surface [15,16,52], at a growth rate of 0.5−1 micron/hour. Note, however, that accurate growth temperature measurement (and comparison among different groups) is not easy. The IR pyrometer, which is typically employed for monitoring the substrate temperature, is often calibrated using the temperature at which oxide desorption starts. However, as it was shown in Ref. [68], the oxide desorption temperature may vary within the range 580−620 °C, depending on the substrate preparation process. Similarly, the phase diagram of surface reconstruction also cannot be a reliable tool to determine accurately the temperature, since it also depends on the substrate heating rate and arsenic pressure. The more accurate optical bandgap measurement is rarely used in high-mobility systems due to the necessity to install additional optical ports near the substrate. Even the accuracy of the As/Ga(Al) beam flux ratio, measured using an ion gauge beam monitor, is limited since it depends on the relative position of the gauge to that of the effusion cells. Therefore, the best growth conditions are usually reached by trial and error.

Special attention should be paid to the process of doping, as described in the previous section. Precautions must be taken to avoid unintentional diffusion or segregation of the dopants (usually Si) towards the 2D electrons region. In the simplest case of uniform or δ-doping, lowering the substrate temperature to 530−560 °C during doping significantly reduces Si diffusion towards the 2D channel (upwards segregation is not important in these structures). The situation, however, is more complicated when dopants are introduced below the 2DEG region. It was shown by Harris et al. [69], using highly sensitive SIMS measurements, that a significant segregation of Si occurs already at a substrate temperature of ~500 °C. Also Pfeiffer et al. [51] found that segregation of Si is the main reason for mobility deterioration in such inverted interfaces. More challenging structures are the DX centre-free SPSL-doped layers, where Si is incorporated in a several-nm-thick GaAs layer (see Figure 6.7d). To avoid the formation of DX centres, the substrate temperature during the doping process must be decreased to 460−480 °C in order to exclude any diffusion and segregation of Si to the AlAs layers. In DHD structures (Figure 6.7e), having normal and inverted interfaces, this requirement is of utmost importance.

It is advisable to keep as many of the system's components, not needed during the growth of a critical layer, cold. For instance, a cracker cell tube should be kept at a low-temperature (~200−400 °C); the silicon effusion cell should be cooled (a filament-like sublimation source may be kept even at room temperature) during growth of the GaAs 2D channel, and heated later either during the spacer growth or during a growth interruption prior to the doped layer.

Growth interruptions are extensively used to facilitate interface smoothness. Thick layers with high AlAs content are often grown as an Al(Ga)As−GaAs supperlattice with growth interruptions after each GaAs layer. According to our experience, in a well-prepared MBE system, even a 60-s long interruption at the critical heterointerface does not result in measurable mobility degradation.

6.6 MOBILITY AND DISORDER IN 2D ELECTRON SYSTEMS

The discovery of quantum Hall effect [1] followed by the observation of the exotic fractional quantum Hall effect [70] demonstrated an exciting behaviour of interacting electrons in two dimensions. The FQHE is a result of a condensation of the 2D electron system into an incompressible quantum fluid, forming many-body ground states with quasiparticle excitations at special values of the Landau-level filling factor $\nu = p/q$ ($\nu = nh/qeB$, with n being the 2DEG areal density, eB/h being the Landau-level degeneracy, and B being the magnetic field). One of the merit factors of the FQHE is the many-body 'energy gap', determined via measuring the activation energy (temperature dependence of longitudinal magnetoresistance R_{xx}). In the early stages of research with samples' mobility $\mu < 5 \times 10^6$ cm^2/V s, a general correlation was established between the mobility and the activation energy [71,72]; however, this relation was not universal. For instance, Sajoto et al. showed in Ref. [7] reasonable FQHE states when the mobility was 3−5 times lower than that reported by Eisenstein et al. [73]. Still the mobility is being used on countless occasions to quantify the disorder in the 2D systems (see for example Ref. [58]).

More comprehensive results were reported by Umansky et al. [3], who studied the behaviour of the magnetoresistance at the 'fragile' 5/2 filling factor in a set of DHD samples containing 2DEG with mobility $\mu \sim 25 \times 10^6 - 36 \times 10^6$ cm^{-2}/Vs embedded in 30 nm wide QWs. An SPSL doping method was employed, while a separate uniformly doped layer was introduced below the surface. With minimal doping density in SPSL (when all the dopants are ionised), the 5/2 state was not established. Moreover, in such samples, no clear correlation between R_{xx} at filling factor 5/2 and the measured mobility was observed. However, introducing spatial correlations among the ionised donors, via precise over-doping, led to a substantial improvement in the robustness of the 5/2 (and similar) states without a notable influence on the mobility. Figure 6.9 shows the dependence of the R_{xx} at the 5/2 state on over-doping, defined via $\gamma = N_D/N_{\mathrm{RI}}^{\mathrm{min}}$, where N_D is the

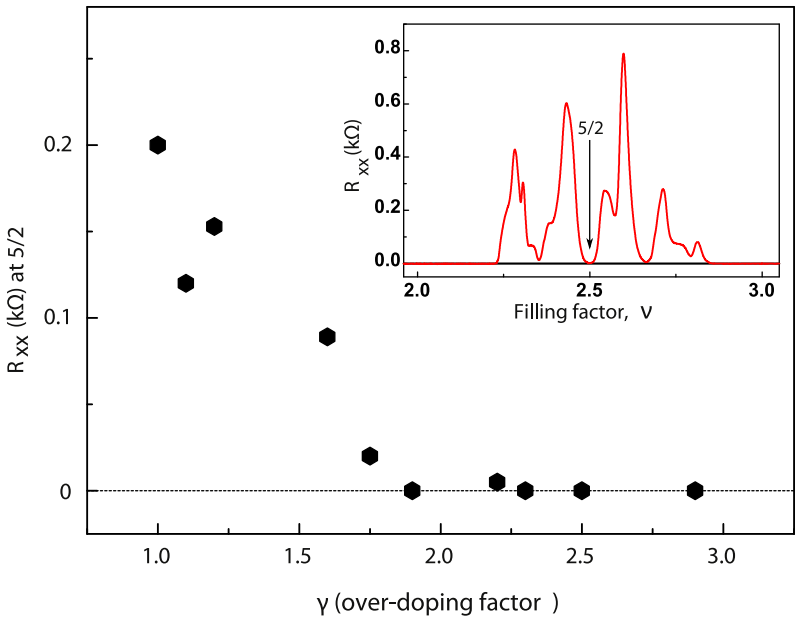

FIGURE 6.9 The longitudinal resistance at filling factor 5/2 measured at T = 10 mK as a function of over-doping in DHD samples with SPSL doping. The 2DEG areal density was ~3×10^{11} cm^{-2} in all samples and the mobility was in the range of 30-36$\times10^{6}$ cm^2/V s. The insert shows a typical magnetoresistance curve (For colour version of this figure, the reader is referred to the online version of this book).

doping density and N_{RI}^{min} is the minimum necessary doping level. An increased γ reduced significantly R_{xx} at $\nu = 5/2$, with an accurate Hall conductance quantisation observed for $\gamma > 2$ at $T = 10$ mK. The upper limit of over-doping $\gamma > 3.5$ was set by the appearance of parallel conduction in the SPSL. Other fractional Hall states behaved similarly, as shown in Figure 6.10. Measuring R_{xx} of the composite fermions (CF) at filling factor $\nu = 1/2$, in a single interface 2D systems with electron densities n_s ~1.2×10^{11}−1.4×10^{11} cm^{-2}, proved, again, that 'smoothing' the disorder potential due to RI leads to a significant improvement in the mobility of the CFs. It should be noted that measurements were done in the dark, the regime, when better temporal stability of mesoscopic devices is generally observed [74].

The high sensitivity of FQHE states to details of the RI potential landscape may be better understood by examining the characteristic scales of the disorder. For BG impurity density of ~1×10^{13} cm^{-3}, the average distance between impurities is ~500 nm; however, their scattering potential, being in the 2DEG region, is 'strong'. On the other hand, the characteristic correlation length of the potential due to RI impurities is determined by the spacer thickness, being $d \sim 60$−100 nm; yet, it is much weaker. It seems that the fractional states are very sensitive to the weaker, though higher spatial frequency, potential fluctuations caused by the RI impurities. This might be related to the actual size of the fractionally charged quasiparticle in comparison with the correlation length of the RI potential [35].

Another approach to induce spatial correlations in the doped layer via over-doping, but still with insignificant parallel conduction, employs a uniform or δ-doping in a low AlAs mole fraction layer $(0.22 < x < 0.3)$. In such layers, the probability to form DX centres is lower; hence, excess doping will result in added neutral donors, with a much lower freeze-out temperature, enabling stronger correlations among D^+ and D^0 states. This type of spatial correlations differs from that in the higher mole fraction AlAs layers $(x > 0.3)$, with 'dipole-like' correlations

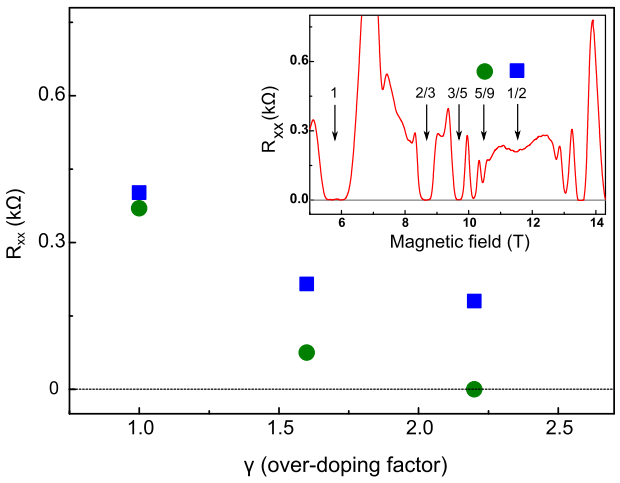

FIGURE 6.10 The longitudinal resistance at filling factors 1/2 (squares) and 5/9 (circles) measured at T = 10 mK as a function of over-doping in SHD samples with SPSL doping. The 2DEG areal density was 1.2×10^{11}−1.4×10^{11} cm^{-2} and the mobility was in the range of 12−17 $\times10^{6}$ cm^2/V s. The insert shows a typical magnetoresistance curve (For colour version of this figure, the reader is referred to the online version of this book).

(DX^- and D^+) as discussed in Section 6.3.4. Despite the fact that a quantitative description of the disorder and its influence on FQHE is not available, the work is continuing with several recent publications confirming the poor correlation between the mobility and the robustness of FQHE states [8,9].

6.7 CONCLUSIONS

Future developments in MBE of high-mobility 2D electron systems, a niche field which supports mostly basic research, are expected to be driven mainly by individuals. The first, and most important goal, is to find a way to purify the source materials further, a process that has already reached its present limits. Moreover, existing high-purity materials characterisation tools have a limited sensitivity, leaving eventually the MBE grower to be the judge of the source material quality. In the realm of MBE system design, one should aim at increasing further the pumping speed with large pumps combined with relatively small chambers that are fully shrouded by LN_2 walls, and possibly even overcooling the LN_2 shrouds.

One of the greatest challenges in structures design as well as in the growth process is control of the disorder landscape. Since the incorporation of doping impurities is random, localising the impurities on a lattice in the plane, hence, correlating them spatially, may be beyond the present technology. However, removing modulation doping, and replacing it by conductive gates that will be employed to induce carriers, seems much more promising. Though previous attempts to operate such devices did not live up to expectations, we believe that with more consorted efforts the disorder in the 2D layer can be minimised.

One should not take lightly the lack of robust temporal stability in mesoscopic devices based on 2D electrons. This crippling effect had been the 'Achilles heel' of most high-mobility structures. The effect is likely to have more than one source, such as: electron hoping among dopants; electron tunnelling among surface states; current leakage from metallic gates and trapped charges in the barrier material, making the problem difficult to solve. Yet, we believe that its origin is more in the growth process rather than in the details of the device fabrication.

Even though much progress had been made in physics that is based on high-mobility 2D electrons, we believe that more physics, waiting to be discovered, is still hiding in even purer materials.

REFERENCES

[1] Klitzing K, von, Dorda G, Pepper M. New method for high-accuracy determination of the fine-structure constant based on quantized Hall resistance. Phys Rev Lett 1980;45:494−7.

[2] Dingle R, Stromer HL, Gossard AC, Wiegmann W. Electron mobilities in modulation-doped semiconductor heterojunction superlattices. Appl Phys Lett 1978;33:665−7.

[3] Umansky V, Heiblum M, Levinson Y, Smet J, Nubler J, Dolev M. MBE growth of ultra-low disorder 2DEG with mobility exceeding $35 \times 10^6\,cm^2/V\cdot s$. J Cryst Growth 2009;311:1658−61.

[4] Schlom DG, Pfeiffer LN. Upward mobility rocks!. Nat Mater 2010;9:881−3.

[5] Watson JD, Mondal S, Csathy GA, et al. Scattering mechanisms in a high-mobility low-density carbon-doped (100) GaAs two-dimensional hole system. Phys Rev B 2011;83:241305.

[6] Prange RE, Girvin SM, editors. The quantum Hall effect. New York: Springer; 1990.

[7] Sajoto T, Suen YW, Engel LW, Santos MB, Shayegan M. Fractional quantum Hall effect in very-low-density GaAs/AlGaAs heterostructures. Phys Rev B 1990;41:8449−60.

[8] Samkharadze N, Watson JD, Gardner G, Manfra MJ, Pfeiffer LN, West KW, et al. Quantitative analysis of the disorder broadening and the intrinsic gap for the 5/2 fractional quantum Hall state. Phys Rev B 2011;84:121305(R).

[9] Pan W, Masuhara N, Sullivan NS, Baldwin KW, West KW, Pfeiffer LN, et al. Impact of disorder on the 5/2 fractional quantum Hall state. Phys Rev Lett 2011;106:20680.

[10] Mooney PM. Deep donor levels (DX centers) in III−V semiconductors. J Appl Phys 1990;67:R1−R26.

[11] Cho AY. Morphology of epitaxial growth of GaAs by a molecular beam method: the observation of surface structures. J Appl Phys 1970;41:2780−6.

[12] Arthur JR. Molecular beam epitaxy. Surf Sci 2002;500:189−217.

[13] Herman MA, Sitter H. Molecular beam epitaxy: fundamentals and current status. Berlin: Springer-Verlag; 1989.

[14] Kubiak RA, Newsfead SM, Sullivan P. The technology and design of molecular beam epitaxy systems. In: Farrow RFC, editor. Molecular beam epitaxy − applications to key materials. William Andrew Publishing/Noyes; 1995.

[15] Pfeiffer L, West KW, Stromer HL, Baldwin KW. Electron mobilities exceeding $10^7\,cm^2/V\cdot s$ in modulation-doped GaAs. Appl Phys Lett 1989;55:1888−90.

[16] Umansky V, de-Picciotto R, Heiblum M. Extremely high-mobility two dimensional electron gas: evaluation of scattering mechanisms. Appl Phys Lett 1997;71:683−5.

[17] Chand Naresh, Harris TD, Chu SNG, Fitzgerald EA, Lopata J, Schnoes M, Dutta NK. Performance of a valved Arsenic cracker source for MBE growth. J Cryst Growth 1993;126:530−8.

[18] Lee K, Shur M, Drummond TJ, Morkoc H. Electron density of the two-dimensional electron gas in modulation doped layers. J Appl Phys 1983;54:2093−6.

[19] Martorel J, Sprung DWL. Determination of the electron density in GaAs/AlGaAs heterostructures. Phys Rev B 1994;49:13750−9.

[20] Davies John H. The physics of low-dimensional semiconductors − an introduction. Cambridge University Press; 1998.

[21] Ando T. Self-consistence results for a GaAs/AlGaAs heterojunction. II. Low-temperature mobility. J Phys Soc Jpn 1982;51:3900−7.

[22] Lee K, Shur MS, Drummond TJ, Morkoc H. Low field mobility of 2-d electron gas in modulation doped $AlxGa_{1-x}As$/GaAs layers. J Appl Phys 1983;54:6432−9.

[23] Walukiewicz W, Ruda HE, Lagowski J, Gatos HC. Electron mobility in modulation-doped heterostructures. Phys Rev B 1984;30:4571−82.
[24] Price PJ. Low temperature two-dimensional mobility of a GaAs heterolayer. Surf Sci 1984;143:145−56.
[25] Hirakawa H, Sakaki K. Mobility of the two-dimensional electron gas at selectivity doped n-type AlGaAs/GaAs heterojunctions with controlled electron concentrations. Phys Rev B 1986;33:8291−303.
[26] Harris JJ, Pals JA, Woltjer R. Electronic transport in low-dimensional structures. Rep Prog Phys 1989;52:1217−66.
[27] Gold A. Mobility of the two dimensional electron gas in AlGaAs/GaAs at low electron densities. Appl Phys Lett 1989;54:2100−2.
[28] Gold A. Temperature dependence of mobility in AlGaAs/GaAs heterostructures for impurity scattering. Phys Rev B 1990;41:8537−40.
[29] Das Sarma S, Hwang EH. Limit to two-dimensional mobility in modulation-doped GaAs quantum structures: How to achieve a mobility of 100 million. Phys Rev B 2008;77:235437.
[30] Lilly MP, Reno JL, Simmons JA, et al. Resistivity of dilute 2D electrons in an undoped GaAs heterostructure. Phys Rev Lett 2003;90:056806.
[31] Laroche D, Das Sarma S, Gervais G, Lilly MP, Reno JL. Scattering mechanism in modulation-doped shallow two-dimensional electron gases. Appl Phys Lett 2010;96:162112.
[32] Saku T, Horikoshi Y, Tokura Y. Limit of electron mobility in AlGaAs/GaAs modulation-doped heterostructures. Jpn J Appl Phys 1996;35:34−8.
[33] Reuter D, Versen M, Schneider MD, Wieck AD. Increased mobility anisotropy in selectively doped AlGaAs/GaAs heterostructures with high electron densities. J Appl Phys 2000;88:321−5.
[34] Harris JJ, Foxon CT, Barnham KWJ, Lacklison DE, Hewett J, White C. Two-dimensional electron gas structures with mobilities in excess of $3 \times 10^6\,\mathrm{cm^2/V \cdot s}$. J Appl Phys 1987;61:1219−21.
[35] Nuebler J, Umansky V, Morf R, Heiblum M, von Klitzing K, Smet J. Density dependence of the $\nu = 5/2$ energy gap: experiment and theory. Phys Rev B 2010;81:035316.
[36] Kawamura T, Das Sarma S. Phonon-scattering-limited electron mobilities in AlGaAs/GaAs heterojunctions. Phys Rev B 1992;45:3612−27.
[37] Efros AL, Pikus FG, Samsonidze GG. Maximum low-temperature mobility of two-dimensional electrons in heterojunctions with a thick spacer layer. Phys Rev B 1990;41:8295−301.
[38] Mycielski J. Formation of a superlattice of ionized resonant donors or acceptors in semiconductors. Solid State Commun 1986;60:165−8.
[39] Buks E, Heiblum M, Shtrikman H. Correlated charged donors and strong mobility enhancement in a two-dimensional electron gas. Phys Rev B 1994;49:14790−3.
[40] Suski T, Wiśniewski P, Dmowski LH, et al. Correlations of the remote impurity charges—a method of 2DEG mobility tuning in GaAs/AlGaAs heterostructures. Solid State Electron 1994;37:677−80.
[41] Wisniewski P, Suski T, Litwin-Staszewska E, Brunthaler G, Kohler K. Mobility and quantum lifetime in a GaAs/AlGaAs heterostructure: tuning of the remote-charge correlations. Surf Sci 1996;361/362:579−82.
[42] Kane BE, Pfeiffer LN, West KW. High mobility GaAs heterostructure field effect transistor for nanofabrication. Appl Phys Lett 1995;67:1262−4.
[43] Harrell RH, Pyshkin KS, Simmons MY, Ritchie DA, Ford CJB, Jones GAC, Pepper M. Fabrication of high-quality one- and two-dimensional electron gases in undoped GaAs/AlGaAs heterostructures. Appl Phys Lett 1999;74:2328−30.
[44] Willett RL, Pfeiffer LN, West KW. Simple-layered high mobility field effect heterostructured two-dimensional electron device. Appl Phys Lett 2006;89:242107−10.
[45] Saku T, Muraki K, Hirayama Y. High-mobility two-dimensional electron gas in an undoped heterostructure: mobility enhancement after illumination. Jpn J Appl Phys 1998;37:L765−7.
[46] Nelson RJ. Long-lifetime photoconductivity effect in n-type GaAlAs. Appl Phys Lett 1977;31:351−4.
[47] Lang DV, Logan RA. Large-lattice-relaxation model for persistent photoconductivity in compound semiconductors. Phys Rev Lett 1977;39:635−9.
[48] Merino EM, editor. DX Centers: donors in AlGaAs and related compounds. Trans Tech Publications Ltd; 1994.
[49] Chadi DJ, Chang KJ. Theory of the atomic and electronic structure of DW centers in GaAs and AlGaAs alloys. Phys Rev Lett 1988;61:873−6.
[50] Vurgaftman I, Meyer JR, Ram-Mohan LR. Band parameters for III−V compound semiconductors and their alloys. J Appl Phys 2001;89:5815−75.
[51] Pfeiffer L, Schubert EF, West KW, Magee CW. Si dopant migration and the AlGaAs/GaAs inverted interface. Appl Phys Lett 1991;58:2258−60.
[52] Saku T, Hirayama Y, Horikoshi Y. High electron mobility in AlGaAs/GaAs modulation-doped structures. Jpn J Appl Phys 1991;30:902−5.
[53] Etienne B, Paris E. Two-dimensional electron gas of very high mobility in planar doped heterostructures. J Physique 1987;48:2049−52.
[54] Baba T, Mizutani T, Ogawa M. Elimination of persistant photoconductivity and improvement of silicon activation coefficient by Al spatial separation from Ga and Si in Al-Ga-As:Si solid system. Jpn J Appl Phys 1983;22:L627−9.
[55] Friedland KJ, Hey R, Kostial H, Klann R, Ploog K. New concept for the Reduction of impurity scattering in Remotely doped GaAs quantum wells. Phys Rev Lett 1996;77:4616−9.
[56] Guha S, Cai Q, Chandrasekhar M, et al. Photoluminescence of short-period GaAs/AlAs superlattices: a hydrostatic pressure and temperature study. Phys Rev B 1998;58:7222−9.
[57] Hikosaka K, Hirachi Y, Mimura T, Abe MA. Microwave-power double-heterojunction high electron-mobility transistor. IEEE Electron Device Lett 1985;6:341−3.
[58] Pfeiffer LN, West KW. The role of MBE in recent quantum Hall effect physics discoveries. Physica E 2003;20:57−64.
[59] Foxon CT, Joyce BA. Interaction kinetics of As_4 and Ga on (100) GaAs surfaces. Surf Sci 1975;50:434−50.
[60] Foxon CT, Joyce BA. Interaction kinetics of As_2 and Ga on (100) GaAs surfaces. Surf Sci 1977;64:293−304.
[61] Ploog K. Molecular beam epitaxy of III−V compounds: technology and growth process. Ann Rev Mater Sci 1981;11:171−210.
[62] Joyce BA. Molecular beam epitaxy. Rep Prog Phys 1985;48:1637−97.

[63] Larkins EC, Harris JS. Molecular beam epitaxy of high quality GaAs and AlGaAs. In: Farrow RFC, editor. Molecular beam epitaxy – applications to key materials. William Andrew Publishing/Noyes; 1995.

[64] Henini M. Molecular beam epitaxy: from research to manufacturing. Thin Solid Films 1997;306:331–7.

[65] Newstead SM, Kubiak RAA, Parker EHC. On the practical applications of MBE surface phase diagrams. J Cryst Growth 1987;81:49–54.

[66] Reginski K, Muszalski J, Preobrazhenskii VV, Lubyshev DI. Static phase diagrams of reconstructions for MBE-grown GaAs(001) and AlAs (001) surfaces. Thin Solid Films 1995;267:54–7.

[67] Baeta Moreira MV, Py MA, Tuncel E. A correlation between surface morphology and RHEED intensity. J Cryst Growth 1991;112:14–26.

[68] SpringThorpe AJ, Ingrey SJ, Emmerstorfer B, Mandeville P, Moore TW. Measurement of GaAs surface oxide desorption temperatures. Appl Phys Lett 1987;50:77–9.

[69] Harris JJ, Bealla RB, Clegga JB, et al. Si migration effects in GaAs/(Al, Ga)As heterojunction and δ-doped structures. J Cryst Growth 1989;95:257–9.

[70] Tsui DC, Stormer HL, Gossard AC. Two-dimensional magnetotransport in the extreme quantum limit. Phys Rev Lett 1982;48:1559–62.

[71] Paalanen MA, Tsui DC, Gossard AC, Hwang JCM. Disorder and fractional quantum Hall effect. Solid State Commun 1984;50:841–4.

[72] Willett R, Stormer HL, Tsui DC, Gossard AC, English JH, Baldwin KW. Fractional quantum Hall effect in extremely high mobility GaAs/(AIGa)As heterostructures. Surf Sci 1988;196:257–62.

[73] Eisenstein JP, Stormer HL, Pfeiffer LN, West KW. Evidence for a spin transition in the ν=2/3 fractional quantum Hall effect. Phys Rev B 1990;41:7910–3.

[74] Dolev M, Heiblum M, Umansky V, Stern Ady, Mahalu D. Observation of a quarter of an electron charge at the 5/2 quantum Hall state. Nature 2008;452:829–34.